Peer reviewed version

University of Bristol - Explore Bristol Research
General rights

The effect of leading edge porosity on airfoil turbulence interaction noise

Luke Bowen,[1, a)] Alper Celik,[2] Beckett Zhou,[1] Michelle Fernandino Westin,[3] and Mahdi Azarpeyvand[1]

[1]*Faculty of Engineering, University of Bristol, Bristol, BS8 1TR,*

United Kingdom

[2]*Aerospace Engineering, Swansea University, Swansea SA1 8EN,*

United Kingdom

[3]*Embraer S.A., São José Dos Campos, SP 12227-901,*

Brazil

(Dated: 6 September 2022)

¹   Airfoil-turbulence interaction noise and the flow-field up to and over the porous lead-

² ing edge is experimentally studied. The porous leading edges were of the same base

³ Triply Periodic Minimal Surface structure with varying porosity to understand how

⁴ the porosity, permeability and pore size affect the generated turbulence interaction

⁵ noise. The turbulent flow was generated by the means of a passive turbulence grid

⁶ which does not affect the normal background noise of the wind tunnel. Far-field

⁷ noise results were obtained from a polar microphone array to assess the directivity

⁸ of the sound as well as the narrowband frequency contributions. Far-field noise re-

⁹ sults demonstrate that increasing porosity reduces the turbulence interaction noise

¹⁰ over low-to-mid frequencies, with a penalty of a high-frequency noise increase. Flow

¹¹ measurement results indicate hydrodynamic penetration of the flow into the porous

¹² structure at the leading edge. Furthermore, the two-point correlation analysis of the

¹³ velocity fluctuations approaching the leading edge, show that the turbulent structures

¹⁴ approaching the solid leading edge appear to deform into more two-dimensional struc-

¹⁵ tures. Whereas, in the case of the porous leading edge the turbulent structures appear

¹⁶ to retain a strong spanwise coherence up to the point of hydrodynamic penetration.

[a] luke.bowen@bristol.ac.uk

I. INTRODUCTION

As noise becomes an ever-increasing environmental concern, turbulence interaction noise is an important phenomenon to be addressed in the drive towards quieter propulsion. Highly rotational, turbulent flows generated by fan blades interact with stator vanes for the purpose of flow straightening. Turbulent structures in the wake of the fan, interact with the leading edge of the stator and subsequent pressure fluctuations on the surface of the airfoil generate noise. The efficiency of noise generation in airfoil turbulence interaction is dictated by the ratio of the size of the turbulent structures, to the leading edge radius of the airfoil.

Turbulence interaction noise is a subject that has been of large social interest since the fundamental study by Amiet[1]. Amiet proposed a model[1] which can predict the interaction noise by implementing linearized airfoil theory to calculate the aerodynamic response of the incident gust on the airfoil; then calculating the unsteady lift propagation to the acoustic far-field accounting for scattering and mean flow effects. Paterson and Amiet[2] showed turbulence impingement as low frequency dominating noise radiation, considering the scale of turbulence is large. Angle of attack effects were studied by Moreau and Roger[3] showing that for noise generation in turbulent flow there is almost no dependency to angle of attack. More commercial type airfoils were studied by Devenport *et al.*[4], where thickness and camber effects of real airfoils were studied for a turbulent flow. Devenport *et al.*[4] concluded that although angle of attack has a strong effect on the airfoil response function, it only has a small effect on noise generation. Varying the turbulent flow has been shown to be just as important as varying the airfoil and this was extensively studied by Hutcheson *et al.*[5].

38 Their tests consisting of a host of different inflow conditions and geometries, finding that as

39 length scale and intensity increased this uniformly increased the spectral levels. Both airfoil

40 geometry and the turbulent inflow are important factors in the noise generation and there

41 have been a host of research on the topic[3,4,6–8], all concluding that the airfoil geometry does

42 in fact alter the noise generation in turbulent flow.

43   Passive noise control techniques have shown to be effective in airfoil noise reduction when

44 implemented to trailing edge configurations[9–15]. Further works have showed the potential

45 of porous materials for noise reduction[9,16–19], but a common conclusion is found that better

46 understanding of the mechanisms and flow interaction is needed to optimize the implemen-

47 tation of porous materials for the noise abatement. As with previous studies[9,10] they found

48 that the porous material will decrease the low frequency noise contribution and increase it at

49 high frequency, suggesting the influence due to surface roughness[20]. Furthermore, turbulence

50 interaction noise has been shown to be reduced by using passive leading edge treatments

51 and in recent years serrated leading edge configurations have gathered much interest[21–25].

52   The reduction of turbulence interaction noise with the use of a porous leading edge has

53 been the subject of much interest[17,26–30]. Sarradj and Geyer were the first to rekindle the

54 interest in porous airfoils and carried out the first study on the effect of a fully porous airfoil[29].

55 The study focused on changing porous properties of airfoils to assess the acoustic benefit,

56 a reduction in noise in most cases was found at the detriment to the overall hydrodynamic

57 performance of the airfoil. Geyer *et al.*[27] studied leading edge noise reduction using fully

58 porous airfoils finding that a reduction in air flow resistivity increases the noise reduction.

59 Geyer *et al.*[16] further developed the porous leading edge idea by adding perforations at the

leading edge of the airfoil, with the remaining chord of the airfoil solid. A noise reduction of up to 8dB was observed and a reduction in the aerodynamic loses compared to the fully porous airfoils. Roger and Moreau[31] used grid generated turbulence to measure the effect that a steel-wool filled NACA 0012 had on noise radiation and showed a maximum of 5dB of noise reduction is achievable from a suboptimal approach. Sinnige *et al.*[19] studied the effect of a flow-permeable perforated leading edge for the reduction of the noise generated on a pylon in the slip-stream of a propeller, in which a measured reduction of the far-field tonal noise was observed. A further step in the characterization of leading edge noise reduction was achieved by Zamponi *et al.*[32] who studied the effect of a porous airfoil on the rapid-distortion of turbulent structures near the leading edge. This experimental and numerical study indicated a reduction in the upwash component of the root-mean-square (rms) of the velocity fluctuation as one of the contributing factors to the reduction of the far-field noise. Chaitanya *et al.*[33] experimentally demonstrated that perforations downstream of the leading edge of a flat plate can reduce the turbulence interaction noise, and used a simple analytic model to show the reduction of noise spectra collapses when plotted against non-demensional frequency. Ocker *et al.*[34,35] demonstrated the noise reduction of a partially porous fan blade, and showed that preserving the solid structure at the leading edge, follow by a porous section immediately downstream can improve both the aerodynamic and aeroacoustic performance. This paper seeks to assess the reduction of airfoil-turbulence interaction noise with porous leading edges of varying porosity. Furthermore, the study considers how the flow approaching and over the leading edge is affected by the introduction of the porous leading edge to offer insight to the noise reduction. The paper is organized as follows: Section II describes the
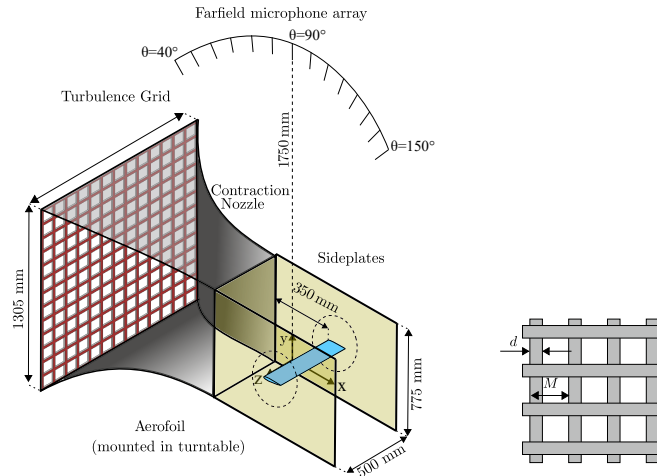
FIG. 1. Schematic of airfoil set-up with turbulence grid and far-field array in the Aeroacoustic Wind tunnel.

wind tunnel, measurement set up porous structure and airfoil. Section III presents the results and discussions of the far-field noise and the velocity field analysis and Section IV concludes this manuscript.

II.   MEASUREMENT SETUP

A.   Wind tunnel and model

The airfoil turbulence interaction noise experiments were performed in the University of Bristol Aeroacoustic Facility, which is a closed-circuit, open-jet anechoic wind tunnel. The chamber has physical dimensions of 6.7 m × 4.0 m × 3.3 m and is anechoic down to 160 Hz[36]. Figure 1 displays a schematic of the wind tunnel contraction with the turbulence grid mounted in the contraction nozzle and the airfoil mounted within sideplates, 350 mm downstream of the contraction nozzle outlet. The contraction nozzle outlet has physical

93 dimensions of 500 mm in width and 775 mm in height, which allows for a steady operation

94 from 5 m/s to 45 m/s and a normal turbulence intensity level below 0.2%[36].

95 This study was conducted with a NACA 0012 profile airfoil that features an interchange-

96 able leading edge which had a span of 600 mm and chord of 200 mm. The airfoil was

97 manufactured in one piece using the additive manufacturing technique of Selective Laser

98 Sintering (SLS) from polyamide. The airfoil was designed to be highly instrumented for

99 the measurement of both aerodynamic and aeroacoustic phenomena in the form of static

100 pressure and unsteady surface pressure. Instrumentation was achieved by the use of brass

101 tubes which were installed with 2 part epoxy resin and smoothed to the surface of the

102 airfoil. In total there were 48 static pressure taps and 88 unsteady surface pressure taps

103 which were drilled with a 0.4 mm bit to avoid pressure attenuation at high frequencies.

104 The surface pressure taps were connected in a remote sensing configuration using Panasonic

105 WM-61A microphones, more information regarding this measurement technique is in the

106 literature[37,38]. All microphones were calibrated in both magnitude and phase referenced to

107 a single GRAS 40PL microphone, which was calibrated using a GRAS 42AA pistonphone

108 calibrator. Unsteady surface pressure measurements made via remote sensing were sam-

109 pled at 2^{15} Hz for 32 seconds. Static pressure measurements were obtained from two Chell

110 MicroDaq-32 pressure acquisition systems and were sampled for 32 seconds at 1000 Hz.

112 **B. far-field measurement**

113 The turbulence interaction noise was measured using the facilities far-field microphone

114 array, see Fig. 1. The array consists of 23 microphones arranged at 5° increments between

TABLE I. Properties of the porous structures used in the leading edge

Porosity, φ (%)	Minimum pore diameter, d_{pore} (mm)	Permeability, κ
40	0.58	2.78×10^{-9}
50	1.48	3.78×10^{-9}
60	2.29	4.98×10^{-9}

115 polar angles of $\theta = 35°$ and $150°$ to allow for directivity measurements. The arc was located

116 1.75 m above the airfoil and the microphone at $90°$ was located directly above the leading

117 edge of the airfoil. The microphones on the arc were 1/4 inch GRAS 40PL microphones,

118 which exhibit a flat frequency response for a large dynamic range of 10 Hz and 20,000 Hz.

119 All microphones were calibrated using a GRAS 42AA pistonphone calibrator prior to the

120 experiments.

121 **C. Turbulence grids**

122 To generate the incoming turbulence, a grid was placed within the contraction nozzle

123 of the wind tunnel, as shown in Fig. 1. The position of the grid within the tunnel was

124 shown to not affect the normal background jet noise of the wind tunnel[39], thus allowing for

125 direct noise measurement of the interaction noise between the turbulent flow and NACA
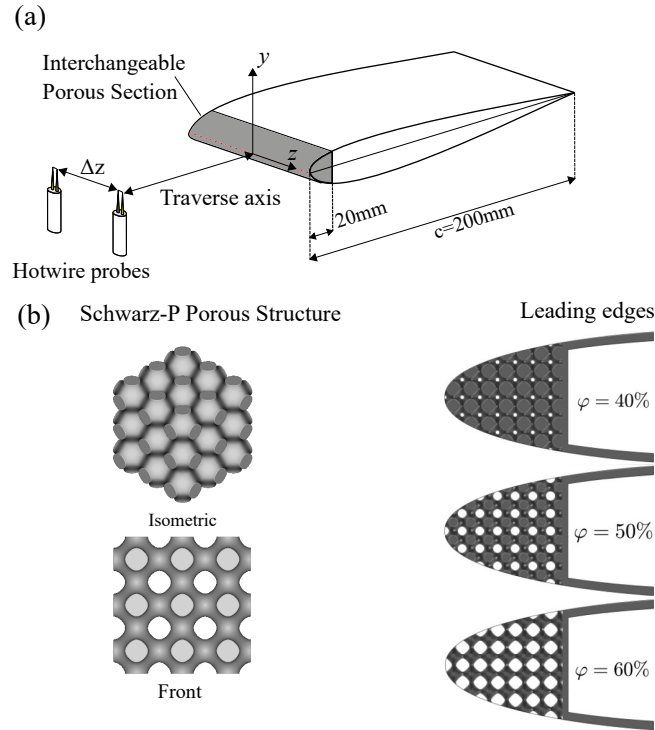
FIG. 2. NACA 0012 airfoil with interchangeable leading edge for both solid and porous leading

edges, schematic of tandem hot-wires and a schematic of the Schwarz-P porous structure.

126 0012 airfoil with various porous leading edges. The geometric properties and generated flow

127 properties of the grid are outlined in Table II.

128 **D. Porous leading edges**

129 Figure 2(a) illustrates a schematic of the airfoil. The first 20% of the leading edge was

130 interchangeable, between a solid, instrumented leading edge and the 3D printed porous

131 leading edges. Three different porous leading edges, with porosity of $\varphi = 40\%$, 50% and

132 60% were selected to study the effect of porosity on the reduction of leading interaction

133 noise. The porous structure is based on the Triply periodic minimal Schwarz-P surface

TABLE II. The geometric properties of the grid, and the flow properties at the position of contraction nozzle exit, $x = 0$, at a freestream velocity $U_\infty = 20$ m/s. The definitions of d and M can be found on Fig. 1.

Diameter, d (mm)	Mesh, M (mm)	σ	Turbulence intensity (%)	Integral length scale (mm)
45	233	0.35	10.1	10.8

134 which occupied the first 10% of the airfoil chord, see Fig. 2(b). The porous leading edge

135 was printed using a FormLabs Form3 stereolithography (SLA) printer. The tested structures

136 were characterized prior to the tests for both porosity and permeability, and are provided

137 in Table I. The porosity of each sample is predefined in CAD software and verified by the

138 mass of the 3D printed structure. The airflow permeability of the structure was defined

139 by measuring the pressure drop across each sample in a permeability rig, a more detailed

140 procedure of this test is previously presented[40].

E. Hot-wire anemometry setup

142 The flow field upstream of and around the leading edge was characterized by Constant

143 Temperature Anemometry (CTA) measurements. Two Dantec 55P16 single-wire probes

144 were used in tandem configuration to obtain two-point correlations in front of the leading

145 edge of the airfoil, as shown in Fig. 2. A Dantec 55P61 minature x-wire probe was utilized

146 to measure the flow field near to the surface of the airfoil leading edge. All probes were

147 operated using a Dantec Streamline Pro system with a CTA91C10 module with a low-

148 pass filter of 30 kHz. The data were acquired using a National Instruments PXIe-4499

149 module mounted in a National Instruments PXIe-1026Q chassis. All hot-wire measurements

150 were sampled at a rate of 2^{15} Hz for a duration of 16 seconds. The data from two-point

151 correlation measurements using tandem hot-wire probes was sampled simultaneously. All

152 hot-wire probes were calibrated daily using a Dantec 54H10 calibrator. Furthermore, the

153 x-wire probe was calibrated for yaw angles between $-40°$ and $40°$. The uncertainty of

154 the velocity measurement was estimated as 2.72% for a free-stream velocity of 20 m/s.

155 The tandem hot-wire probes, used for spanwise coherence studies, were traversed using a

156 ThorLabs LTS300 300 mm Translation Stage with stepper motor along the x-axis with a

157 positioning accuracy of ± 5 μm. The tandem probes were arranged along the z-axis directly

158 upstream of the airfoil leading edge, see Fig. 2b. The probes were traversed upstream of the

159 airfoil leading edge to acquire measurements at 35 streamwise locations covering the region

160 -100 mm$< x < -0.03$ mm, corresponding to $-31.51 < x/r < -0.01$, where r is the leading

161 edge radius of the airfoil. Two-point correlations for a broad range of separation distances

162 were obtained with repeated traverse measurements with the separation distance ranging

163 between 5.3 mm $< z < 27$ mm, corresponding to $1.67 < \Delta z/r < 6.40$. The x-wire probe

164 was traversed using two connected ThorLabs LTS300 for movement in both the x-axis and
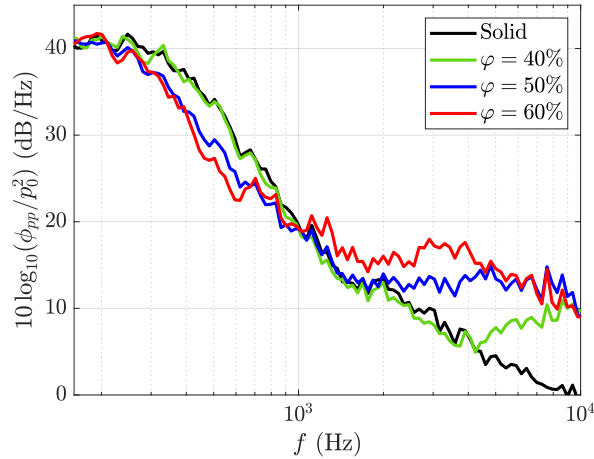
165 y-axis.

FIG. 3. Far-field noise generated by the NACA 0012 airfoil with a solid and porous leading edge immersed in the turbulent flow generated by the grid and measured by the microphone at $\theta = 90°$ directly above the leading edge.

III. RESULTS

A. Far-field noise analyses

The far-field noise of the NACA0012 airfoil with solid and porous leading edges in the flow generated by a turbulence grid are presented in this section. The presented results are for a single flow velocity of $U_\infty = 20$ m/s, with a turbulence intensity of 10.1% and integral length scale of $\Lambda = 10.8$ mm. The section considers the power spectral density level (PSD) of the far-field noise observed at different polar angles, see Fig. 1, over the frequencies 160 Hz$< f < 10,000$ Hz. This is calculated using $10 \cdot \log_{10}(\phi_{pp}/p_0^2)$, where ϕ_{pp} is the power spectral density of the measured acoustic pressure and p_0 is the reference pressure of 20 μPa. Secondly, the overall sound pressure level is presented and the directivity of the radiated
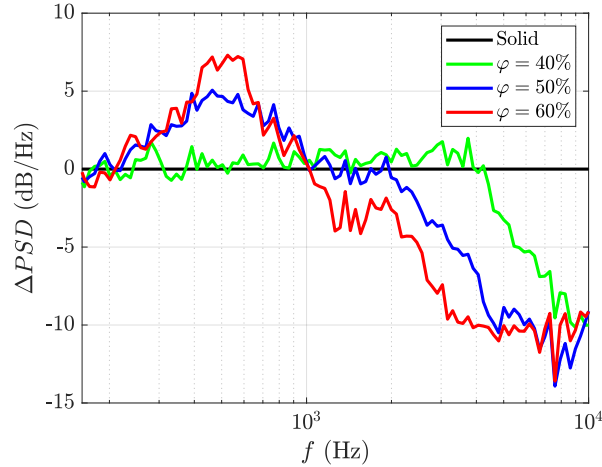
FIG. 4. Comparison of the Far-field noise reduction obtained by each porous leading edge compared to the solid leading edge immersed in the turbulent flow generated by the grid and measured by the microphone at $\theta = 90°$ directly above the leading edge.

176 noise is considered. The overall sound pressure level is calculated as,

$$OASPL = 10 \cdot \log_{10} \left[\frac{\int \phi_{pp}(f)\, \mathrm{d}f}{p_0^2} \right], \tag{1}$$

177 integrating the energy spectrum with respect to frequency, between 160 Hz$< f < 20,000$

178 Hz. It should be noted that the turbulence interaction noise of the airfoil is significantly

179 higher than the normal background noise of the wind tunnel jet between the frequencies 160

180 Hz $< f < 1000$ Hz. For frequencies between 1000 Hz $< f < 10,000$ Hz interaction noise is

181 not observed, and the airfoil noise generated by the NACA0012 airfoil is comparable to the

182 background noise of the facility. Both observations are previously demonstrated[39].

183   First, we consider the airfoil turbulence interaction noise measured by the microphone

184 on the array at polar $\theta = 90°$, positioned directly above the leading edge. Figure 3 shows

185 the comparison between the noise spectra of the NACA0012 airfoil with a solid and porous
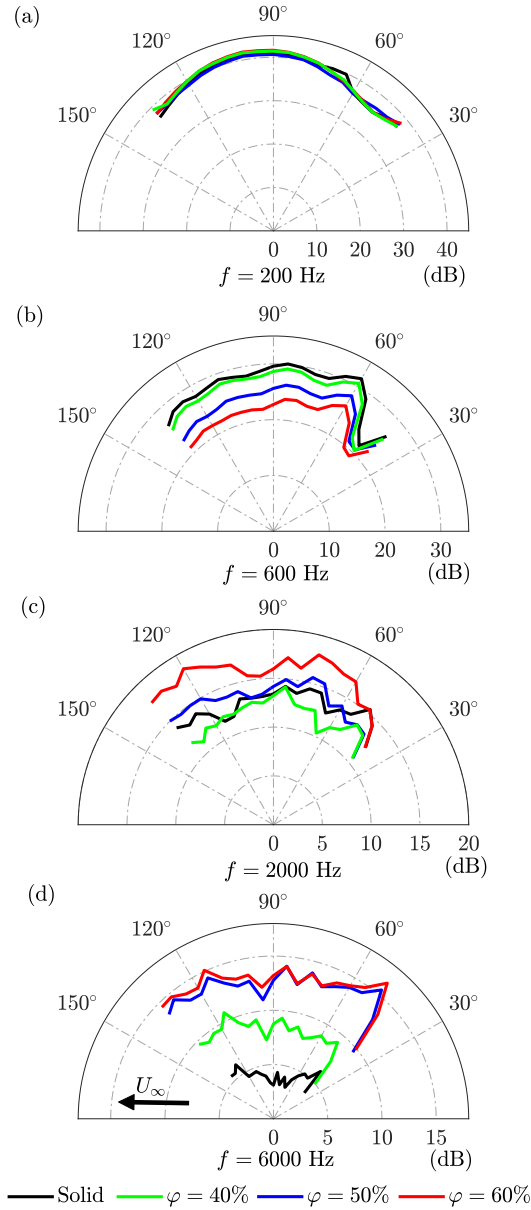
13

FIG. 5. Directivity of PSD level of the noise for the solid and porous leading edge cases measured by the microphone array and presented for frequencies (a) $f = 200$ Hz, (b) $f = 600$ Hz, (c) $f = 2000$ Hz and (d) $f = 6000$ Hz.

186 leading edges, plotted against narrowband frequency. When comparing the results of the

187 porous leading edges to those of the solid leading edge, it can be seen that porosity plays

14

188 an important role on the level of noise reduction that is achieved. Considering the results of

189 the leading edge of porosity $\varphi = 40\%$, there is little-to-no noise reduction over the frequency

190 range where turbulence interaction noise is observed, i.e. 160 Hz $< f <$ 1000 Hz. An

191 increase in the porosity of the leading edge results in a reduction of the observed turbulence

192 interaction noise, where the greatest reduction is for the $\varphi = 60\%$ leading edge. The

193 results show that increasing the porosity of the leading edge structure can further reduce

194 the turbulence interaction noise. However, it is clear from Fig. 3 that the porous leading

195 edge results also demonstrate a noise increase at higher frequencies i.e. $f >$ 1000 Hz. An

196 increase in the porosity of the leading edge structure enhances the high frequency noise

197 generation. This high frequency noise generation is previously shown to be caused by the

198 flow interacting with the rough porous structure[20] and can be reduced with the introduction

199 of a cover over the porous material[41]. Although the high frequency noise increase in the

200 case of the porous leading edge results is significant compared to the results of the solid

201 airfoil leading edge, the noise increase is observed at a much lower PSD level than the noise

202 reduction.

203   A clearer performance of the noise reduction achieved by each porous leading edge is

204 provided by Fig. 4, where the far-field noise data is presented as $\Delta PSD = PSD_{solid} -$

205 PSD_{porous} and a positive value denotes noise reduction. As can be seen in Fig. 4, the use

206 of a $\varphi = 60\%$ porous treatment can lead to a noise reduction of up to 7 dB over 400 Hz

207 $< f <$ 700 Hz. Observed noise reduction for the leading edge with a porous treatment of

208 $\varphi = 50\%$ peaks at 5 dB for the frequency range 400 Hz $< f <$ 600 Hz. Furthermore, both

209 leading edges of porosity $\varphi = 60\%$ and $\varphi = 50\%$ demonstrate noise reduction between 160

210 Hz $< f <$ 1000 Hz. Interestingly, the porous leading edge of porosity $\varphi = 40\%$ shows no

211 significant noise reduction over 160 Hz $< f <$ 4000 Hz. High frequency noise increase is

212 evident in the results of each porous leading edge, however the frequency of where the noise

213 increase is evident varies with porosity.

214 To assess the potential changes to the mechanism that causes the turbulence interaction

215 noise as a result of employing porous leading edges, the directivity of the sound at multiple

216 frequencies has been considered. A significant change to the directivity patterns between

217 the solid and porous cases may signify a change to the noise generation mechanism. Figure

218 5 presents the results of the directivity of the PSD level for the solid and porous leading

219 edge cases at four chosen frequencies, namely $f = 200$ Hz, 600 Hz, 2000 Hz and 6000

220 Hz, at a freestream velocity of $U = 20$ m/s. The frequencies were chosen to cover the low

221 frequencies (160 Hz$< f <$ 1000 Hz), where turbulence interaction is dominant, the cross-over

222 frequency ($f = 2000$ Hz), where little or no noise change was observed, and high frequencies

223 (2000 Hz$< f <$ 10,000 Hz), where the significant noise increase due to surface roughness is

224 observed. The results of directivity of the radiated noise for $f = 200$ Hz are presented in

225 Fig. 5(a) and demonstrate no change in the directivity pattern between the solid and porous

226 leading edge cases. At the frequency $f = 600$ Hz, the results show a reduction of up to 7 dB

227 in the radiated noise from the airfoils fitted with a porous leading edge. Between the polar

228 angles $60° < \theta < 135°$, the reduction of the PSD becomes more substantial as the porosity

229 increases, although there is little change to the pattern of the radiated noise. Furthermore,

230 Between polar angles $40° < \theta < 60°$ there is less significant reduction of the PSD between

231 the results of the solid and porous leading edges. At the crossover frequency ($f = 2000$ Hz),

16

232 the directivity pattern of the solid and porous cases exhibit some differences, despite the

233 comparable levels of PSD exhibited in Figs. 3 and 4. At high frequencies, i.e. $f = 6000$

234 Hz, where the roughness noise is believed to be the dominant noise source in the case of the

235 porous leading edges, the directivity patterns are significantly different to that of the solid

236 leading edge, signifying the changes to the noise generation mechanism.

237 The overall sound pressure level (OASPL) results assesses the directivity pattern of the

238 noise generated by the solid and porous leading edge cases. As the OASPL calculation

239 integrates the PSD level across the narrowband spectrum, the OASPL results include each

240 porous leading edge's contribution to the low frequency noise reduction and the subse-

241 quent noise increase at higher frequencies too. Figure 6 presents the OASPL results of the

242 NACA0012 airfoil turbulence interaction noise with solid and porous leading edges at a

243 freestream velocity of $U = 20$ m/s. The directivity results of the solid and porous leading

244 edges are comparable across the polar angles presented. The maximum level of OASPL noise

245 reduction is approximately 3 dB and is achieved by the leading edge of porosity $\varphi = 60\%$,

246 between the polar angles of $65° < \theta < 100°$. It is clear that when considering the full

247 noise spectrum, the reduction of the turbulence interaction noise achieved using the porous

248 leading edge far outweighs the roughness noise increase observed at high frequency, see Fig.

249 4. Considering the OASPL results of the solid case compared to the porous cases, it is clear

250 that the leading edge with porosity $\varphi = 40\%$ shows little noise reduction. Interestingly, both

251 the result of $\varphi = 50\%$ and $\varphi = 60\%$ demonstrate comparable results for OASPL. Aside from

252 the reduction in the porous cases, there is no significant change to the directivity pattern

253 between the cases.

254 It is understood from the assessment of the far-field noise that the introduction of a

255 porous leading edge reduces the turbulence interaction noise generated by the airfoil. To

256 understand the physical mechanism responsible for the reduction of the far-field noise, the

257 flow field upstream of and around the airfoil must be examined.
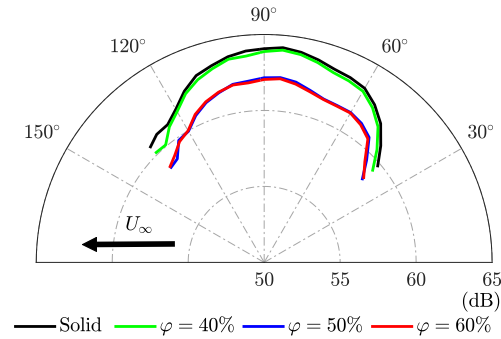

FIG. 6. Directivity of the OASPL for the NACA 0012 airfoil with both solid and porous leading
edges.

258 **B.   Flow field analyses**

259 Detailed flow measurements of the region in front of and around the leading edge of the

260 airfoil were carried out to quantify flow field differences between the solid and porous leading

261 edges, using single-wire and two-component x-wire hotwire probes. Flow field analyses are

262 presented for a grid flow with a turbulence intensity of 10.1% and integral length scale of

263 $\Lambda = 10.8$ mm, at the free-stream velocity of $U_\infty = 20$ m/s. Figure 7 presents the vectors

264 of velocity results for the solid and porous leading edge cases for a freestream velocity of

265 $U_\infty = 20$ m/s. Each arrow is representative of the resultant velocity vector, measured

18

266 by the x-wire probe at each location. The results of the solid case demonstrate the flow

267 deflection caused by the airfoil near the leading edge (i.e. $-0.01 < x/c < 0.05$) and the

268 velocity vectors following the airfoil shape further downstream of the leading edge (i.e.

269 $0.05 < x/c < 0.25$). The velocity results in the vicinity of the surface of the airfoil shows

270 no significant difference to the magnitude of the arrows further from the airfoil surface,

271 signifying that the measurements for the solid case are taken outside the boundary layer.

272 The results of the porous leading edge cases show that the flow penetrates into the porous

273 leading edge region, represented as the arrows near the leading edge with a lower vertical

274 velocity component (i.e. more horizontal). The flow penetration into the porous leading edge

275 is more evident in the region $-0.01 < x/c < 0.1$. The main differences between the flows

276 of each case are evident in the vectors closest to the surface of the airfoil, where increased

277 porosity generates a larger velocity deficit close to the surface. This result helps to highlight

278 the flow penetration into the porous leading edges which a single-wire probe is unable to

279 capture.

280   As previously shown[32,42], the flow structures undergo significant changes in close proxim-

281 ity of the stagnation point, before impinging on the airfoil. Given the spatial constraint, and

282 also need for resolving high frequencies, such flow measurements can only be achieved using

283 single-wire probes. Detailed flow measurements upstream of the airfoil leading edge, ob-

284 tained with the use of a single-wire hotwire probe, reveal interesting behavior for the porous

285 leading edge cases in the vicinity of the leading edge (i.e. $-1.5 < x/r < -0.01$). Figure

286 8 presents the results of velocity measurements upstream of the leading edge of the solid

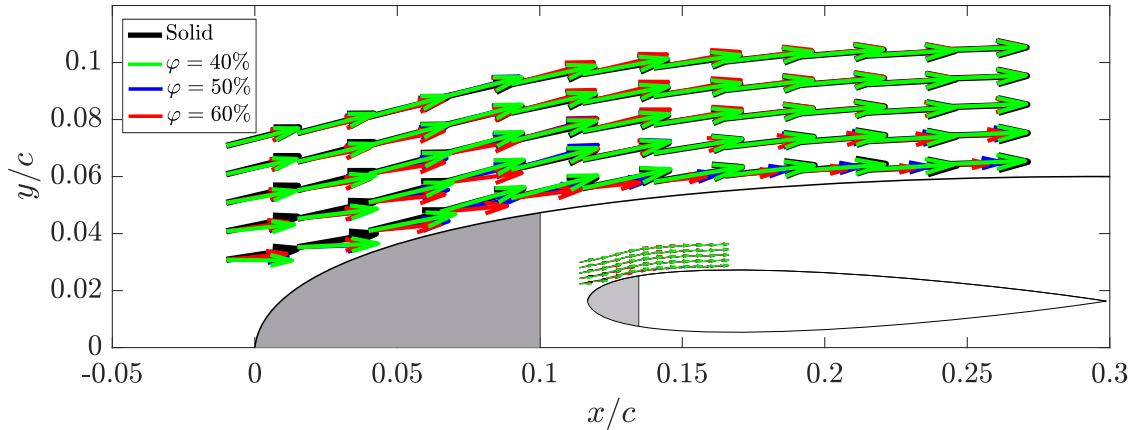287 and porous airfoil leading edges over a wide spacial range, i.e. $-5 < x/r < -0.01$. Figure

FIG. 7.   Vectors of velocity magnitude over the leading edge region of the airfoil for both the solid and porous leading edge case measured by CTA cross-wire probe.

288   8(a) presents the mean-flow velocity normalized by the freestream velocity (U/U_∞) for the

289   solid and porous leading edge cases. The mean-flow velocity results of the solid leading edge

290   demonstrate a reduction in the velocity approaching the leading edge of the airfoil, caused

291   by the velocity stagnation of the solid airfoil leading edge. This result is expected and con-

292   sistent with the literature[32]. When comparing the solid and porous leading edges results,

293   all results demonstrate comparable behavior for the region $-5 < x/r < -1.5$. In the case

294   of solid leading edge, the stagnation effect is evident by a sharp decay in the total velocity

295   along the stagnation streamline between $-1.5 < x/r < -0.01$. However, the stagnation

296   effect for the porous leading edges is dramatically reduced, which signifies the presence of

297   flow penetration into the porous volume. It should be noted that unlike the solid leading

298   edge results, there is an acceleration of the flow close to the porous leading edges which is

299   exacerbated by decreasing porosity.

300   Turbulence interaction with an external body can cause significant changes to the tur-

301 bulence intensity of the flow in the proximity of the body[32,42]. The presence of a porous

302 structure and potential flow penetration into the porous volume can further complicate the

303 evolution of the turbulent structures upstream of the external body. Figure 8(b) presents the

304 root-mean-square (rms) of the velocity fluctuation normalized by the rms of freestream veloc-

305 ity fluctuation for both the solid and porous leading edge cases. The results of the solid lead-

306 ing edge demonstrate a reduction in the rms of velocity fluctuation approaching the leading

307 edge within $-5 < x/r < -0.25$. In proximity to the leading edge, i.e. $-0.25 < x/r < -0.01$,

308 there is a sudden increase in the velocity fluctuation which is caused by redistribution of

309 the velocity fluctuation from the streamwise direction to the crosswise, known as upwash[32].

310 Comparing the results of the solid and porous cases, again, a comparable behavior is ob-

311 served for the region $-5 < x/r < -1.5$. In the region where the solid leading edge results

312 experiences a reduction, followed by a sudden recovery of the rms of velocity fluctuation,

313 the porous leading edges results demonstrate a significant increase in the rms of velocity

314 fluctuations, inside $-1.5 < x/r < -0.01$. As shown in Fig. 8(b), in the case of the solid

315 leading edge, the rms of velocity fluctuation reaches its minimum at $x/r = -0.15$, while

316 that for the $\varphi = 60\%$ has moved to the location $x/r = -0.8$. The position of the minimum

317 value of rms of velocity fluctuation moves further upstream from the leading edge as the

318 porosity decreases. For $\varphi = 60\%$, 50% and 40% the location of the rms of velocity increase

319 is $x/r \approx -0.8$, -1 and -1.5, respectively. Furthermore, as porosity decreases, the level of

320 the velocity fluctuation rms at the leading edge significantly increases. This is an interesting

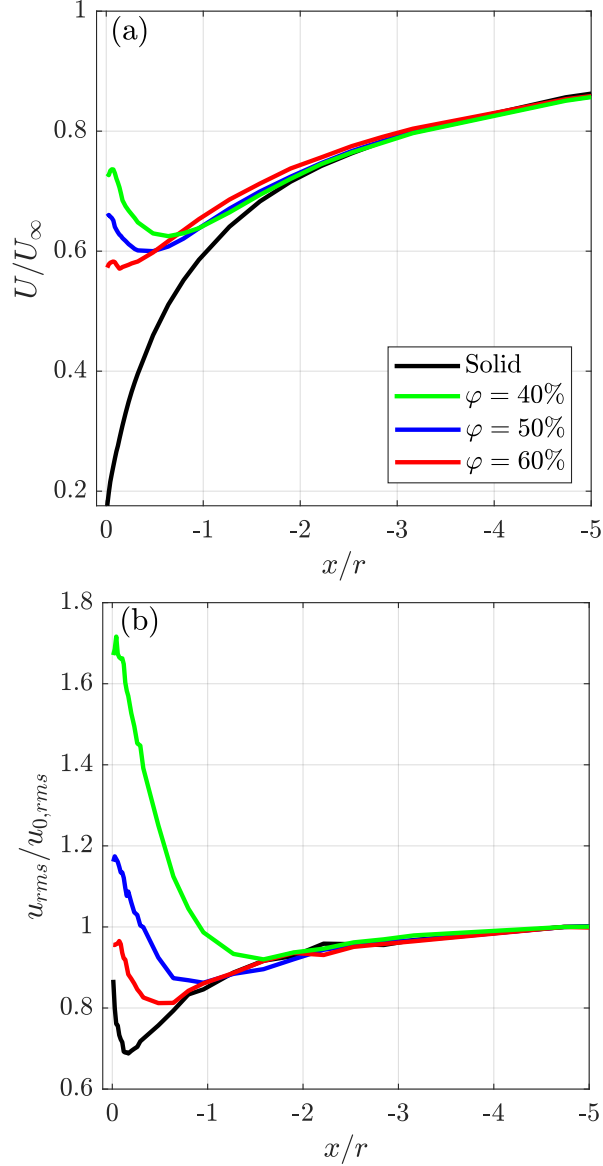321 result, and contrasts to the previous observation in the literature[32].

FIG. 8.   Stagnation streamline flow properties measured by single-wire probe for *(a)* normalized flow velocity (U/U_∞) and *(b)* normalized velocity fluctuation ($u_{rms}/u_{0,rms}$) for the solid and porous leading edge cases.

322   To understand the energy content of the velocity fluctuations along the stagnation stream-
323   line, the power spectral density level of the velocity fluctuations has been calculated and
324   is presented in two forms. The first, is the standard presentation that is used as an input

325 for noise prediction models i.e. Amiet[1], which is the PSD level of the velocity fluctuations,

326 calculated as $10 \log_{10}(\phi_{uu}/u_{0,rms}^2)$. The second, is the pre-multiplied energy spectra, where

327 the pre-multiplied energy spectra is presented and the total area under the curve is rep-

328 resentative of the total energy at each location. The remaining results presented in this

329 paper are a comparison between the solid case and the porous leading edge of porosity

330 $\varphi = 50\%$ for the sake of brevity. Figures 9(a) and 9(c) presents the PSD level of velocity

331 fluctuations for the solid and porous leading edge cases and figures 9(b) and 9(d) presents

332 the pre-multiplied energy spectra of velocity fluctuations for the solid and porous leading

333 edge cases. The PSD level of velocity fluctuations results for the solid case demonstrate an

334 interesting behavior. At the freestream measurement location, there is a consistent value

335 of PSD level of velocity fluctuation, a turning point at $f = 60$ Hz, and a consistent decay

336 gradient of $f^{-5/3}$ between 100 Hz$< f <$ 2000 Hz signifying freely-decaying turbulence of the

337 inertial subrange. Up to $x/r = -0.33$, there is a reduction in the low frequency content in

338 the PSD of velocity fluctuation (i.e. $f <$ 100 Hz), coupled with a reduction at very high

339 frequency (i.e. $f >$ 2000 Hz). However, no change to the $f^{-5/3}$ decay range is observed. In

340 proximity of the leading edge $(-0.15 < x/r < -0.01)$, there is a recovery to the low fre-

341 quency energy content of the velocity fluctuation, accompanied by a reduction of the velocity

342 energy contact at high frequencies. When comparing the PSD level of velocity fluctuation

343 along the stagnation streamline for the solid and porous leading edge, see figures 9(a) and

344 9(c), a more apparent change in both the low and high frequency behavior is evident in

345 the porous leading edge case. The dissimilarity of the PSD of velocity fluctuations between

346 the results of the solid and porous leading edge cases are more evident in the region close

23

³⁴⁷ to the leading edge, i.e. $-0.96 < x/r < -0.01$. The low frequency increase in the PSD

³⁴⁸ of velocity fluctuations, evident within $-0.33 < x/r < -0.01$, exceeds the low frequency

³⁴⁹ levels measured at the freestream, i.e. $x/r = -33$. Furthermore, there is an emergence of

³⁵⁰ a broadband hump which peaks at $f = 70$ Hz. When considering the high frequency decay

³⁵¹ gradients, the results of the solid case show no significant deviation from the $f^{-5/3}$ decay

³⁵² gradient between the frequency range 100 Hz$< f < 2000$ Hz. However, velocity PSD results

³⁵³ for the porous leading edge case show the high frequency decay gradient increases along

³⁵⁴ the stagnation streamline approaching the leading edge. The change to the high frequency

³⁵⁵ decay of the velocity fluctuation is a significant observation as this phenomenon signifies

³⁵⁶ external contribution to the change of the small scale turbulent structures approaching the

³⁵⁷ porous leading edge.

³⁵⁸ The pre-multiplied energy spectra accentuates the variations between the cases as the

³⁵⁹ total area under each curve is representative of total energy and are presented in Figs. 9(b)

³⁶⁰ and 9(d). The pre-multiplied energy spectra results offer more insight into the nature of

³⁶¹ the velocity fluctuation along the stagnation streamline, presented in Fig. 8. The pre-

³⁶² multipled energy spectra results for the solid leading edge show the reduction of energy

³⁶³ up to $x/r = -0.15$ and sudden recovery at $x/r = -0.01$ is more clear. The pre-multiplied

³⁶⁴ energy spectra of velocity fluctuation results of the solid leading edge appear to lose more low

³⁶⁵ frequency energy up to $x/r = -0.15$, as the peak of the curve reduces and shifts to a higher

³⁶⁶ frequency. At the stagnation point, $x/r = -0.01$, there is some recovery of the velocity

³⁶⁷ fluctuation energy level but it remains lower than that of the freestream flow $(x/r = -33)$.

³⁶⁸ As can be seen in Fig. 9(d), the porous leading edge results are dramatically different from

369 those of the solid case. It is clear in the results of the pre-multipled energy spectra that

370 the behavior far upstream of the leading edge, i.e. $x/r = -4.74$ and -0.96, is comparable

371 between the solid and porous cases. Closer to the leading edge, at $x/r = -0.33$, the energy

372 level of the velocity fluctuations remain comparable to that of the freestream level, but with

373 the emergence of a distinct peak at about $f = 70$ Hz. In the proximity of the leading edge

374 $(x/r = -0.01)$, the energy level is seen to further increase around $f = 70$ Hz, with the most

375 energetic turbulent scales concentrated between 40 Hz$< f < 300$ Hz.

376   The energy spectra data presented here provides insight to the energy level of the flow

377 structures for the solid and porous leading edge cases, showing significant dissimilarities

378 between the cases in close proximity to the leading edge. However, we still need to gain an

379 understanding of the physical size and changes to the shape of the turbulent structures as

380 the approaching the airfoil leading edge, this is further explored in the next section with the

381 analysis of two-point correlation upstream of the leading edge.

382   **C.   Two-point correlation analysis**

383   The two-point correlation of the velocity fluctuations along the stagnation streamline,

384 schematically illustrated in Fig. 2, offers information on the level of coherence of the flow

385 structures and their physical size in the spanwise direction. By performing several two-probe

386 coherence studies at different streamwise locations upstream of the leading edge, one can

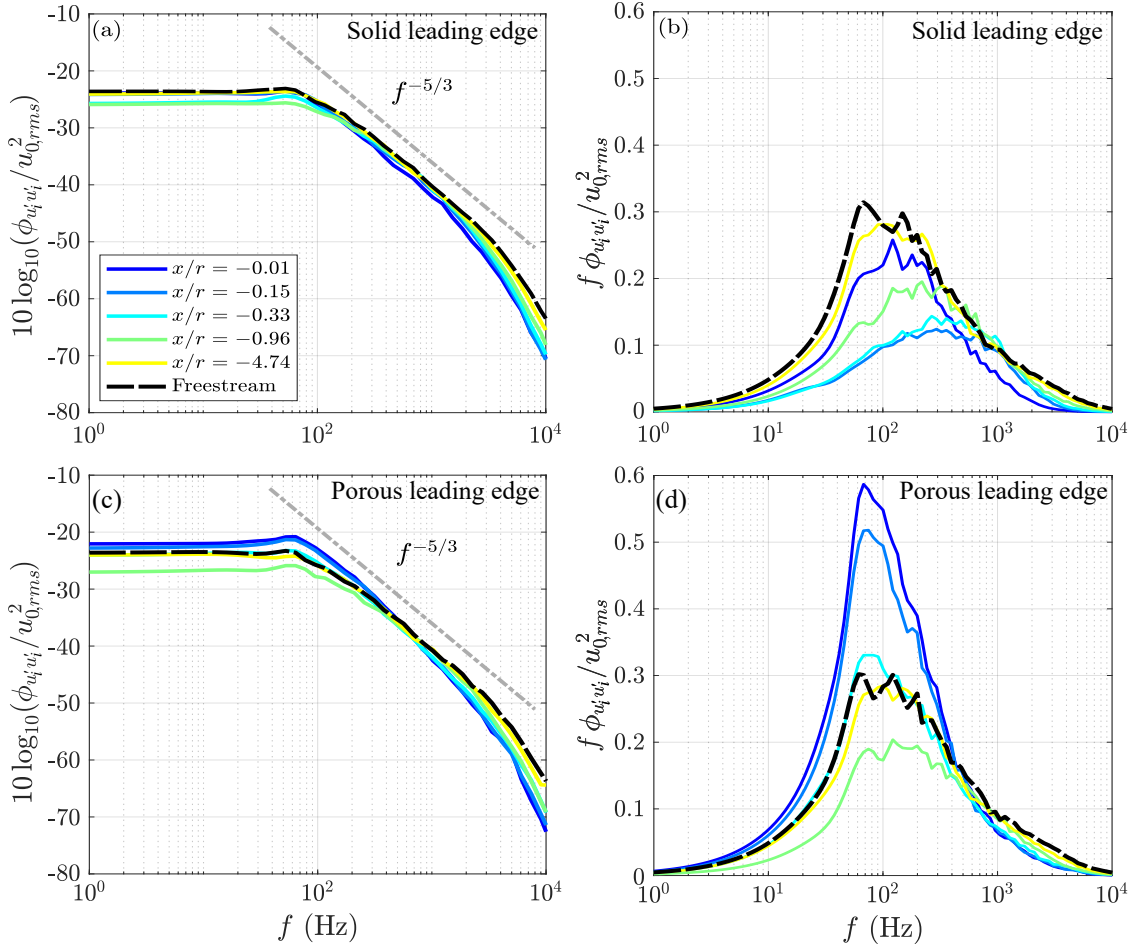387 study the changes to the size of the turbulent flow structures as they approach the airfoil

FIG. 9. Energy spectrum analysis of velocity fluctuation along the stagnation streamline upstream of the NACA 0012 aerofoil leading edge between $-4.74 < x/r < -0.01$ where (a) and (c) are the PSD and pre-multiplied PSD of the solid leading, (b) and (d) are the PSD and pre-multiplied PSD of the porous leading edge ($\varphi = 50\%$).

leading edge. The magnitude-squared of the spanwise coherence is calculated as

$$\gamma^2_{u'_i u'_j}(f, \Delta z) = \frac{\left|\phi_{u'_i u'_j}(f)^2\right|}{\left|\phi_{u'_i u'_j}(f)\right|\left|\phi_{u'_i u'_j}(f)\right|}, \tag{2}$$

where $\gamma^2_{u'_i u'_j}(f, \Delta z)$ is the spanwise coherence calculated between two single-wire probes in a tandem configuration, separated by Δz, and $\phi_{u'_i u'_j}$ denotes the cross-power spectral density between the two probes i and j, respectively. Figure 10 presents the results of the spanwise

coherence of the velocity fluctuation for the flow along the stagnation streamline for the case

with the solid leading edge at different upstream locations (freestream, $x/r = -4.74$, -0.96,

-0.33, -0.15 and -0.01), and for a wide range of probe separations ($\Delta z/r = 6.40$, 4.16,

2.68, 2.11, and 1.67). Considering the spanwise coherence results for the freestream case

(Fig. 10(a)), there appears to be a strong level of coherence at frequencies 10 Hz$< f < 100$

Hz, for small spanwise separation distance ($\Delta z/r = 1.67$), which steadily decays up to

$f = 1000$ Hz. The level of coherence at low frequency (i.e. $f < 1000$ Hz) systematically

decreases as the spanwise separation increases to $\Delta z/r = 6.40$. At the far upstream location

$(x/r = -4.74)$, see Fig. 10(b), there is still a high level of spanwise coherence of the

velocity fluctuation evident, although there is a reduction in the magnitude, particularly at

the highest spanwise separation ($\Delta z/r = 6.40$). As seen, the results at the far upstream

locations ($x/r = -4.74$) in Fig. 10(b), are very similar to those observed in the freestream

cases in Fig. 10(a). In Fig. 10(c), a further reduction in the level of spanwise coherence of

velocity fluctuation is evident at $x/r = -0.96$, however there is still sensitivity to the increase

of spanwise separation. At locations closer to the leading edge, up to $x/r = -0.33$, there is

an overall reduction in the spanwise coherence of the velocity fluctuations, and the coherence

becomes less dependent on the spanwise spacing (Δz), indicating the emergence of more two-

dimensional flow structures. Approaching the stagnation, at $x/r = -0.15$, the coherence

begins to increase, compared to $x/r = -0.33$. The coherence level further increases in the

imminent upstream region of the leading edge between $x/r = -0.15$ and $x/r = -0.01$.

Furthermore, there is the emergence of a dominant peak in the spanwise coherence of the

velocity fluctuation for all separations which is centered at $f \approx 70$ Hz. As mentioned

414 earlier, the sensitivity of the two-point velocity coherence to spanwise separation distance

415 (Δz) is gradually lost moving towards the airfoil leading edge which can be interpreted

416 as the turbulent structures becoming more two-dimensional. This behavior represents the

417 turbulent structures distorting and rolling up over the leading edge of the airfoil.

418   Figure 11 presents the results of the spanwise coherence of the velocity fluctuations for

419 the flow along the stagnation streamline between $-4.74 < x/r < -0.01$ for the case with the

420 porous leading edge. As the same turbulent flow is generated in both leading edge cases, the

421 freestream results for the solid and porous cases are the same. As previously shown in Fig.

422 8, the results of the velocity and rms of velocity fluctuation for the solid and $\varphi = 50\%$ porous

423 leading edges exhibit the same behavior between $-4.74 < x/r < -0.96$. This is echoed in

424 the spanwise coherence results for the same region, as the same results are evident for the

425 solid case (Figs. 10(b) and (c)) as in the porous case (Figs. 11(b) and (c)), respectively.

426 For the porous leading edge case there is a reduction in the spanwise coherence approaching

427 $x/r = -0.96$ which corroborates with the results of the solid leading edge. Moving close to

428 the leading edge ($x/r = -0.33$), disparities in the coherence results between the solid and

429 porous leading edge cases appear inside one leading edge radius of the leading edge, i.e. Figs

430 10(d) and 11(d), as the spanwise coherence of the velocity fluctuations begin to increase.

431 The level of spanwise coherence of velocity fluctuations is more significant for the porous

432 than that of the solid case. While the coherence results of the porous case show some

433 level of spanwise distance dependency, this is weaker than the freestream turbulent flow

434 further upstream, indicating the emergence of more two-dimensional turbulent structures in

435 the vicinity of the leading edge. In the proximity of the leading edge, i.e. $x/r = -0.01$,

the level of spanwise coherence of the velocity fluctuation further increases to exceed the freestream level for all separations. In addition, the dominant peak of $f \approx 70$ Hz, evident in Figs. 9(c) and 9(d), remains a prominent feature for all spanwise separation distances at $x/r = -0.01$. The higher level of coherence coupled with the increased energy level of the turbulent structures at close proximity to the leading edge demonstrates that the porous leading edge significantly changes the behavior of the flow close to the leading edge of the airfoil.

The flow field and two-point correlation analyses demonstrate how a turbulent flow upstream of the airfoil leading edge can be altered by the introduction of the porous treatment over the leading edge area. Furthermore, the variation in the leading edge porosity between $\varphi = 40\%$ and $\varphi = 60\%$ is shown to result in strong changes to the energy content of the velocity fluctuations upstream of the leading edge. However, it should be noted that the presented results only cover a single turbulent inflow condition. The underlying physics of turbulence interaction noise is believed to be dependent on the turbulent characteristics of the inflow, specifically the turbulent intensity and integral length scale[2,5,39]. To this end, the physics of the noise reduction mechanism for a porous leading edge in airfoil turbulence interaction noise is likely susceptible to the turbulent inflow conditions. Future works will focus on better understanding of flow distortion around porous leading edges in turbulent flows with a range of turbulence intensities and integral length scales.

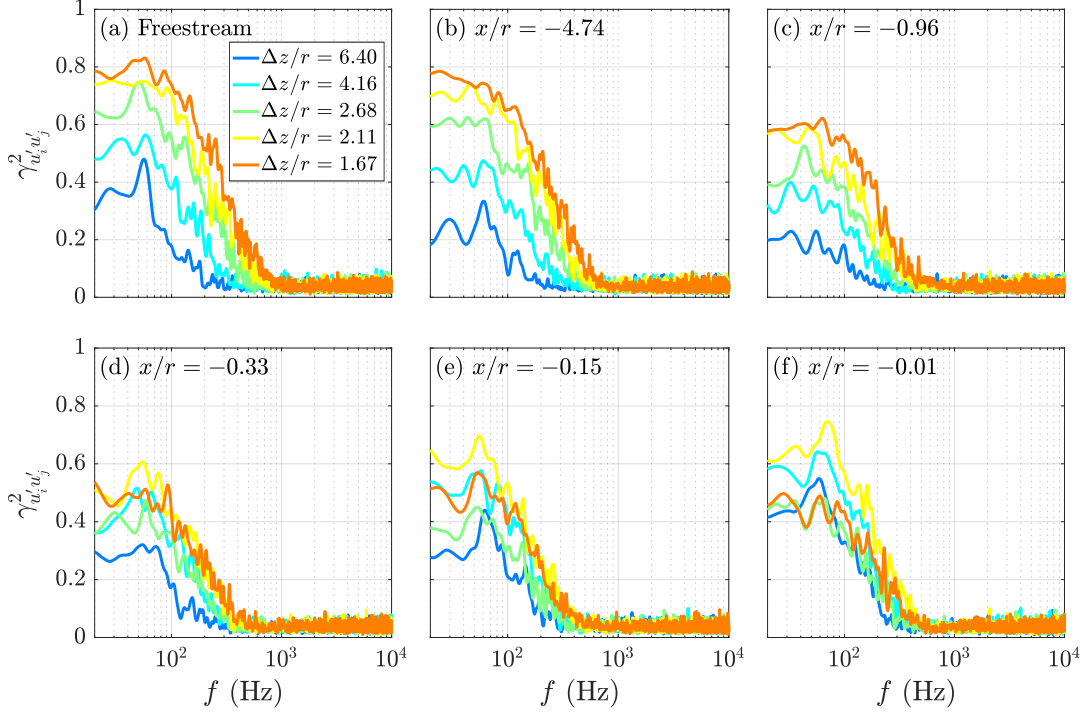FIG. 10. Spanwise magnitude-square coherence $(\gamma^2_{u'_i u'_j})$ of velocity fluctuation measured by tandem hot-wire probes at multiple spanwise separations $(\Delta z/r)$ for solid leading edge along stagnation streamline.

IV. CONCLUSION

This paper presents a study on airfoil turbulence interaction noise reduction using a porous treatment at the leading edge. The study implements a NACA 0012 airfoil of chord $c = 200$ mm which interacts with a turbulent flow, generated by the means of a passive turbulence grid. The leading edge part of the airfoil is interchangeable between a solid leading edge and a porous leading edge. The structure utilized at the leading edge is a Schwartz-Primitive Triply periodic minimal structure. The porosity of the leading edge is varied between three values of porosity $\varphi = 40\%$, 50% and 60% to alter the bulk materials'

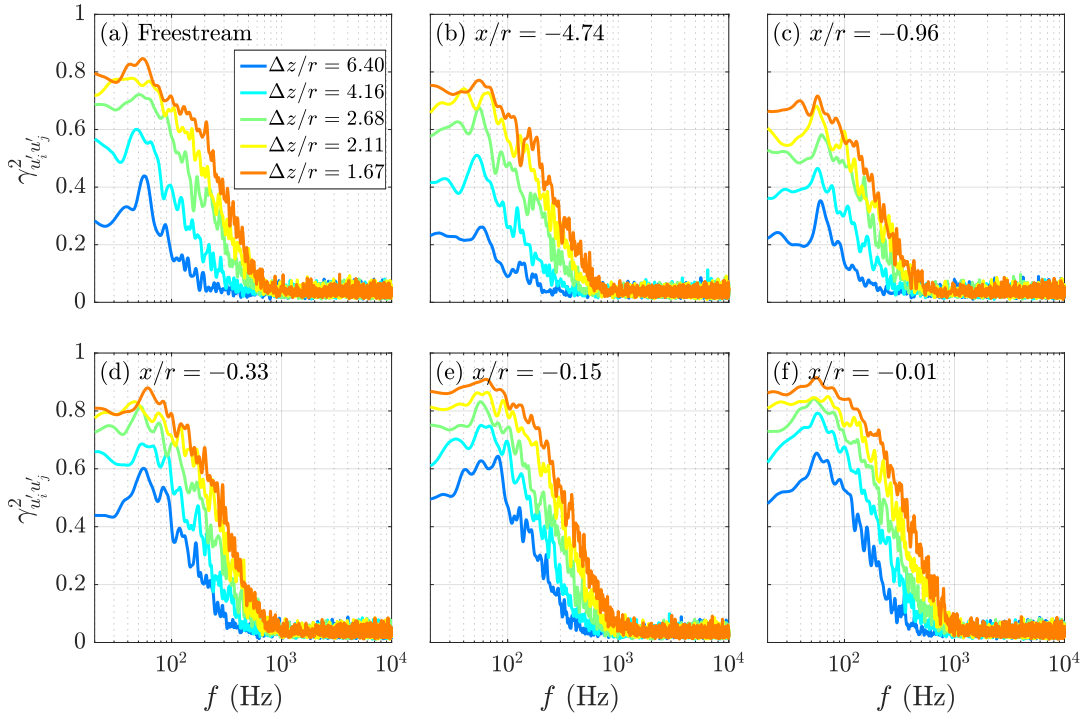FIG. 11. Spanwise magnitude-square coherence $(\gamma^2_{u'_i u'_j})$ of velocity fluctuation measured by tandem hot-wire probes at multiple spanwise separations $(\Delta z/r)$ for porous leading edge $(\varphi = 50\%)$ along the stagnation streamline.

permeability. Variation of the porosity and permeability of the leading edges was studied to understand their effect on turbulence interaction noise. Far-field noise results suggested that increasing the porosity results in more effective low-frequency noise reduction, with the penalty of high-frequency noise increase. The use of a porous leading edge with a porosity of $\varphi = 40\%$ showed little noise reduction compared to the solid leading edge, whereas 50% and 60% demonstrated significant noise reduction at low frequencies. The overall sound pressure level results revealed little variation in the directivity of the noise between the solid and porous leading edges, and the overall sound pressure level results

471 between the $\varphi = 50\%$ and 60% cases offer comparable noise reduction. Analysis of the

472 flow field by the means of CTA hot-wire measurements revealed flow penetration into the

473 porous leading edges, with increasing porosity showing a velocity deficit close to the wall

474 of the airfoil. An interesting behavior is observed for measurements along the stagnation

475 streamline, when approaching the leading edge of the airfoil a rapid increase in the rms of

476 velocity fluctuation is evident, contrary to previous experimental observations. The analysis

477 of the PSD of velocity fluctuations confirmed a significant increase in the energy level close

478 to the porous leading edge which contradicts the current experimental literature. Further

479 numerical and experimental investigations are needed to understand whether the increase

480 in energy is due to the redistribution of energy from streamwise to crosswise, or due to the

481 nature of the hydrodynamic penetration of the flow in the porous leading edge. Two-point

482 spanwise velocity fluctuations coherence analysis revealed that approaching the leading edge

483 of the airfoil the solid case generates a 2D structure due to the loss of separation sensitivity

484 between the hotwires. For the porous leading edge, it is evident that spanwise coherence of

485 the velocity fluctuations increases near the porous leading edge and exceeds the freestream

486 level.

EP/S013024/1 at the University of Bristol from 1/6/2020 to 1/12/2022. All authors would like to acknowledge the financial support of EPSRC via Grant No. EP/S013024/1.

REFERENCES

[1]R. Amiet, "Acoustic radiation from an airfoil in a turbulent stream," Journal of Sound and Vibration **41**(4), 407 – 420 (1975) doi: https://doi.org/10.1016/S0022-460X(75)80105-2.

[2]R. Paterson and R. Amiet, "Acoustic radiation and surface pressure characteristics of an airfoil due to incident turbulence," Proceedings of the 3rd Aeroacoustics Conference, Palo Alto, CA, AIAA-76-571 (1976).

[3]S. Moreau and M. Roger, "Effect of angle of attack and airfoil shape on turbulence-interaction noise," 11th AIAA/CEAS Aeroacoustics Conference, Monterey, CA, AIAA-2005-2973 (2005).

[4]W. J. Devenport, J. K. Staubs, and S. A. Glegg, "Sound radiation from real airfoils in turbulence," Journal of Sound and Vibration **329**(17), 3470 – 3483 (2010) doi: https://doi.org/10.1016/j.jsv.2010.02.022.

[5]F. V. Hutcheson, T. F. Brooks, and D. J. Stead, "Measurement of the noise resulting from the interaction of turbulence with a lifting surface," International Journal of Aeroacoustics **11**(5-6), 675–700 (2012) doi: 10.1260/1475-472X.11.5-6.675.

[6]J. Gill, X. Zhang, and P. Joseph, "Symmetric airfoil geometry effects on leading edge noise," The Journal of the Acoustical Society of America **134**(4), 2669–2680 (2013) doi:

511   10.1121/1.4818769.

512   [7]J. R. Gill, X. Zhang, and P. Joseph, "Effects of real airfoil geometry on leading edge gust

513   interaction noise," 19th AIAA/CEAS Aeroacoustics Conference, Berlin, Germany AIAA-

514   2013-2203 (2013), doi: 10.2514/6.2013-2203.

515   [8]J. Gershfeld, "Leading edge noise from thick foils in turbulent flows," The Journal of the

516   Acoustical Society of America **116**(3), 1416–1426 (2004) doi: 10.1121/1.1780575.

517   [9]S. A. Showkat Ali, M. Azarpeyvand, and C. R. Ilário da Silva, "Trailing-edge flow and

518   noise control using porous treatments," Journal of Fluid Mechanics **850**, 83–119 (2018)

519   doi: 10.1017/jfm.2018.430.

520   [10]S. A. Showkat Ali, M. Azarpeyvand, and C. R. I. da Silva], "Trailing edge bluntness noise

521   reduction using porous treatments," Journal of Sound and Vibration **474**, 115257 (2020)

522   doi: https://doi.org/10.1016/j.jsv.2020.115257.

523   [11]X. Liu, H. K. Jawahar, M. Azarpeyvand, and R. Theunissen, "Aerodynamic performance

524   and wake development of airfoils with serrated trailing-edges," AIAA Journal **55**(11),

525   3669–3680 (2017).

526   [12]Y. D. Mayer, B. Lyu, H. K. Jawahar, and M. Azarpeyvand, "A semi-analytical noise

527   prediction model for airfoils with serrated trailing edges," Renewable Energy **143**, 679 –

528   691 (2019) doi: https://doi.org/10.1016/j.renene.2019.04.132.

529   [13]H. K. Jawahar, Q. Ai, and M. Azarpeyvand, "Experimental and numerical investigation

530   of aerodynamic performance for airfoils with morphed trailing edges," Renewable Energy

531   **127**, 355 – 367 (2018) doi: https://doi.org/10.1016/j.renene.2018.04.066.

[14] A. Celik, Y. Mayer, and M. Azarpeyvand, "An experimental aeroacoustic study on serrated trailing-edge geometries and flow misalignment effects," AIAA AVIATION 2020 FORUM, AIAA-2020-2518 (2020).

[15] A. Celik, Y. D. Mayer, and M. Azarpeyvand, "On the aeroacoustic characterization of a robust trailing-edge serration," Physics of Fluids **33**(7), 075120 (2021) doi: 10.1063/5.0054767.

[16] T. F. Geyer, A. Lucius, M. Schrödter, M. Schneider, and E. Sarradj, "Reduction of turbulence interaction noise through airfoils with perforated leading edges," Acta Acustica united with Acustica **105**(1), 109–122 (2019) doi: doi:10.3813/AAA.919292.

[17] M. Roger, C. Schram, and L. D. Santana, "Reduction of airfoil turbulence-impingement noise by means of leading-edge serrations and/or porous material," 19th AIAA/CEAS Aeroacoustics Conference, Berlin, Germany, AIAA-2013-2108 (2013).

[18] A. R. Carpio, F. Avallone, and D. Ragni, "On the role of the flow permeability of metal foams on trailing edge noise reduction," 2018 AIAA/CEAS Aeroacoustics Conference, Atlanta, GA, AIAA-2018-2964 (2018).

[19] T. Sinnige, B. D. Corte, R. De Vries, F. Avallone, R. Merino-Martínez, D. Ragni, G. Eitelberg, and L. L. M. Veldhuis, "Alleviation of propeller-slipstream-induced unsteady pylon loading by a flow-permeable leading edge," Journal of Aircraft **56**(3), 1214–1230 (2019) doi: 10.2514/1.C035250.

[20] S. A. Showkat Ali, M. Azarpeyvand, M. Szőke, and C. R. Ilário da Silva, "Boundary layer flow interaction with a permeable wall," Physics of Fluids **30**(8), 085111 (2018) doi:

553   10.1063/1.5043276.

554   [21]B. Lyu, M. Azarpeyvand, and S. Sinayoko, "Noise prediction for serrated leading-edges,"

555   22nd AIAA/CEAS Aeroacoustics Conference, Lyon, France, AIAA-2016-2740 (2016).

556   [22]B. Lyu and M. Azarpeyvand, "On the noise prediction for serrated leading edges," Journal

557   of Fluid Mechanics **826**, 205–234 (2017) doi: 10.1017/jfm.2017.429.

558   [23]J. Kim, S. Haeri, and P. Joseph, "On the reduction of aerofoil-turbulence interaction noise

559   associated with wavy leading edges," Journal of Fluid Mechanics **792**, 526–552 (2016).

560   [24]S. Narayanan, C. Paruchuri, S. Haeri, P. Joseph, J. W. Kim, and C. Polacsek, "Airfoil

561   noise reductions through leading edge serrations," Physics of Fluids **27**(2), 025109 (2015)

562   doi: 10.1063/1.4907798.

563   [25]C. Paruchuri, P. Joseph, S. Narayanan, C. Vanderwel, J. Turner, J. W. Kim, and B. Gana-

564   pathisubramani, "Performance and mechanism of sinusoidal leading edge serrations for the

565   reduction of turbulence-aerofoil interaction noise," Journal of Fluid Mechanics **818**, 435–

566   464 (2017) doi: 10.1017/jfm.2017.141.

567   [26]K. N. Chanaud, R. and R. Sitterding, "Experiments on porous blades as a means of

568   reducing fan noise," Journal of the Acoustical Society of America **59**, 564–575 (1976).

569   [27]T. Geyer, E. Sarradj, J. Giesler, and M. Hobracht, "Experimental assessment of the noise

570   generated at the leading edge of porous airfoils using microphone array techniques," 17th

571   AIAA/CEAS Aeroacoustics Conference (32nd AIAA Aeroacoustics Conference), Portland,

572   OR, AIAA-2011-2713 (2011).

[573] [28]T. Geyer, E. Sarradj, and J. Giesler, "Application of a beamforming technique to the measurement of airfoil leading edge noise," Advances in Acoustics and Vibration **2012**, 1–16 (2012) doi: 10.1155/2012/905461.

[576] [29]E. Sarradj and T. Geyer, "Noise generation by porous airfoils," 13th AIAA/CEAS Aeroacoustics Conference (28th AIAA Aeroacoustics Conference), AIAA-2007-3719 (2007).

[578] [30]R. Zamponi, N. V. de Wyer, and C. F. Schram, "Experimental investigation of airfoil turbulence-impingement noise reduction using porous treatment," 25th AIAA/CEAS Aeroacoustics Conference, Delft, Netherlands, AIAA-2019-2649 (2019).

[581] [31]M. Roger and S. Moreau, "Airfoil turbulence-impingement noise reduction by porosity or wavy leading-edge cut: Experimental investigations," INTER-NOISE and NOISE-CON Congress and Conference Proceedings **253**(2), 6366–6375 (2016).

[584] [32]R. Zamponi, S. Satcunanathan, S. Moreau, D. Ragni, M. Meinke, W. Schröder, and C. Schram, "On the role of turbulence distortion on leading-edge noise reduction by means of porosity," Journal of Sound and Vibration **485**, 115561 (2020) doi: https://doi.org/10.1016/j.jsv.2020.115561.

[588] [33]C. Paruchuri, P. Joseph, T. P. Chong, M. Priddin, and L. Ayton, "On the noise reduction mechanisms of porous aerofoil leading edges," Journal of Sound and Vibration (2020) doi: j.jsv.2020.115574.

[591] [34]C. Ocker, F. Czwielong, T. F. Geyer, P. Chaitanya, M. Merkel, and S. Becker, "Permeable structures for leading edge noise reduction," AIAA AVIATION 2021 FORUM, AIAA-2021-2192 (2021).

[35] C. Ocker, T. F. Geyer, F. Czwielong, F. Krömer, W. Pannert, M. Merkel, and S. Becker, "Permeable Leading Edges for Airfoil and Fan Noise Reduction in Disturbed Inflow," AIAA Journal **59**(12), 4969–4986 (2021) doi: 10.2514/1.J060396.

[36] Y. D. Mayer, H. K. Jawahar, M. Szőke, S. A. S. Ali, and M. Azarpeyvand, "Design and performance of an aeroacoustic wind tunnel facility at the university of bristol," Applied Acoustics **155**, 358 – 370 (2019) doi: https://doi.org/10.1016/j.apacoust.2019.06.005.

[37] A. P. G. Sagrado, "Boundary layer and trailing edge noise sources," Ph.D. Thesis, University of Cambridge (2008).

[38] Y. Mayer, B. Zang, and M. Azarpeyvand, "Near-field aeroacoustic characteristics of a stalled naca 0012 aerofoil," in *Proceedings of the 23rd International Congress on Acoustics, integrating 4th EAA Euroregio 2019*, edited by M. Ochmann, Proceedings of the ICA AND EAA EUROREGIO, DEGA e.V. (2019), pp. 5421–5428.

[39] L. Bowen, A. Celik, M. Azarpeyvand, and C. R. I. da Silva, "Grid generated turbulence for aeroacoustic facility," AIAA Journal **60**(3), 1833–1847 (2022) doi: 10.2514/1.J060851.

[40] L. Bowen, A. Celik, M. Azarpeyvand, and C. R. da Silva, "Porous geometry effects on the generation of turbulence interaction noise," in *AIAA AVIATION 2021 FORUM,AIAA 2021-2193*, doi: 10.2514/6.2021-2193.

[41] L. Bowen, A. Celik, M. Azarpeyvand, and C. R. I. da Silva, "On the use of tailored permeable surfaces for turbulence interaction noise control," AIAA AVIATION 2020 FORUM, AIAA-2020-2530 (2020).

615 [42]L. D. Santana, J. Christophe, C. Schram, and W. Desmet, "A rapid distortion theory

616 modified turbulence spectra for semi-analytical airfoil noise prediction," Journal of Sound

617 and Vibration **383**, 349–363 (2016) doi: https://doi.org/10.1016/j.jsv.2016.07.026.